THE GENERATION OF TOXIC REACTIVE OXYGEN SPECIES (ROS) FROM MECHANICALLY ACTIVATED SULFIDE CONCENTRATES AND THE EFFECT ON THERMOPHILIC BIOLEACHING

Gavin C. Jones[a]*, Kirsten C. Corin[b], Robert P. van Hille[a] and Susan T.L. Harrison[a]

[a]Centre for Bioprocess Engineering Research,
[b]Centre for Minerals Research,
Department of Chemical Engineering, University of Cape Town,
Private Bag, Rondebosch 7701, South Africa. *Email: Gavin.Jones@uct.ac.za

Abstract

In this study two types of laboratory mills, planetary and vibratory, were used to mechanically activate both pyrite and chalcopyrite concentrates to differing extents via milling. These samples were first analysed by particle size, surface area, density, scanning electron microscopy and XRD line profile analysis. Secondly, reactivity in solution was measured in terms of the generation of toxic reactive oxygen species (ROS) hydrogen peroxide and hydroxyl radicals. The ROS generation from milled sulfides, normalised at a constant surface area loading, were found to increase simultaneously with increased mechanical activation (*i.e.* milling time). Increased ROS generation was postulated to be caused by a combination of increased surface area defects and bulk particle-related defects measured after samples were subjected to milling. The measured ROS generation profiles showed that planetary milled samples generated significantly more ROS per sample surface area compared to vibratory milled samples. Thermophilic bioleaching tests were conducted to investigate the effect of mechanical activation on bioleaching performance. Brief periods of mechanical activation (2.5 – 10 min) improved leach performance, relative to unactivated feed, up to a certain specific surface area loading (m^2/L), determined for each concentrate. Poor bioleaching performance resulted from samples subjected to prolonged periods of mechanical activation (20 – 60 min). Planetary milled samples were less amenable to bioleaching. For intensively milled samples, a complete lack of inoculated cells was observed, via fluorescent microscopy, a few days after inoculation, suggesting culture death had occurred. The generation of toxic ROS from mechanically activated fine sulfide particles was postulated to be the cause for poor bioleaching performance.

Keywords: Sulfide ores, fine milling, mechanochemistry, bioleaching

1. Introduction

The effect of sulfide concentrate re-grinding on the performance of tank biooxidation or bioleaching systems is not clearly understood despite being widely practised in industry. Some hydrometallurgical advantages of mechanically activating concentrates via fine milling include increased leach rates, increased metal extraction efficiencies and decreased pulp retention times (Baláž, 2003; Baláž *et al*., 2004). Table 1 shows typical P_{80} re-grind particle sizes of tank biooxidation and bioleaching process and the typical pulp density (PD) used. Finer grind sizes have been found to be essential for efficient copper recovery, particularly from chalcopyrite containing sulfide concentrates used in the BioCop and BacTech/Mintek processes. Reprocessing of sulfide tailings for the economic recovery of residual valuable metals, especially gold and cobalt (Kasese Cobalt), is becoming an increasing trend in tank bioleaching technologies. Therefore there is greater opportunity for implementation of re-grinding circuits as a specific process step for sulfide mechanical activation. This warrants research on the influence of selection and operation of re-grinding mills to maximise process performance.

Table 1. Typical pulp densities (PD) and product re-grind sizes for sulfide biooxidation and bioleaching processes (Rawlings *et al* ., 2003; Dreisinger, 2009; Watling, 2008)

Process	PD [w/w%]	P_{80} re-grind [µm]	Metal of interest
Bacox	16.3	45	gold
Biox	20	75	gold
Kasese Cobalt	20	35	cobalt/nickel
BioNic	17.5	75	nickel
BioCop	12	37	copper
BacTech/Mintek	14.2	10	copper

The mechano-chemically induced changes of milled sulfide particles can be measured at the surface (Murphy and Strongin, 2009) and in the whole volume or bulk of particles with a variety of analytical techniques. Studies performed on mechanical activation of sulfide particles have shown a relationship between changes measured at both the surface and the bulk of particles, mostly due to the semi-conductive properties of most sulfides. Changes due to solid state chemical transformation such as the conversion of crystalline mineral to other products and the overall deformation of crystal structures (crystallites) present in the bulk of the particles have also become a focus, especially with prolonged periods of mechanical activation for the specific synthesis of nanomaterials (Baláž and Dutková, 2009). The link between upstream re-grinding of sulfide concentrates and the downstream biohydrometallurgical processing has been focused largely on particle size reduction, with little reference to mechanical activation. New technologies are emerging that specifically employ ultrafine milling of copper and nickel sulfide concentrates (Activox and Nenatech), followed by atmospheric, low pressure or temperature oxidative leaching (Baláž and Dutková, 2009). Here the increased sulfide feed amenability or reactivity is attributed to the generation of new mineral surface area and the reduction of bulk particle crystallinity, resulting in improved leach performance. To exploit sulfide reactivity in a biohydrometallurgical context, re-grinding of sulfide particles is only beneficial where the

concentration of reaction products formed in solution from reacting sulfide surfaces remain within the limits of the physiological tolerances of bioleaching micro-organisms. The reactivity of pyrite, contained within coal samples, on exposure to aqueous solution has been studied with respect to the generation of toxic reactive oxygen species (ROS) such as hydrogen peroxide (H_2O_2), superoxide anion radicals $(O_2^{\bullet})^-$ and hydroxyl radicals ($^{\bullet}OH$) (Cohn *et al*., 2006). The formation of ROS at pyrite particle surfaces has been attributed to the iron-catalysed Haber-Weiss reactions (Rxn 1 and 2). The H_2O_2 formed can react with Fe (II) in solution to form $^{\bullet}OH$ via the Fenton reaction (Rxn 3):

py-Fe (II) + O_2	→	Fe (III) + $(O_2^{\bullet})^-$	(Rxn 1)
py-Fe (II) + $(O_2^{\bullet})^-$ + $2H^+$	→	Fe (III) + H_2O_2	(Rxn 2)
Fe (II) + H_2O_2	→	$^{\bullet}OH$ + OH^- + Fe (III)	(Rxn 3)

Another mechanism has been characterised for pyrite induced ROS generation in solution (Schoonen *et al*., 2006; Borda *et al*., 2003) where surface adsorbed water molecules can form $^{\bullet}OH$ at intrinsic or mechanically-induced surface defects (Rxn 4) present as sulfur deficient iron sites. It is possible for H_2O_2 to be formed from two reacting $^{\bullet}OH$ (Rxn 5):

py-Fe (III) + H_2O	→	py-Fe (II) + $^{\bullet}OH$ + H^+	(Rxn 4)
2 $^{\bullet}OH$	→	H_2O_2	(Rxn 5)

ROS is particularly toxic to cellular life. Free radicals such as $^{\bullet}OH$ and $(O_2^{\bullet})^-$ react indiscriminately with biomolecules at rates limited by diffusion (Imlay, 2008). When a free radical reacts with a non-radical, it produces another free radical, initiating a chain reaction. If left unchecked, these chain reactions can disrupt an entire cell through the deactivation of enzymes, destruction or mutation of DNA and the disruption of the cell membrane resulting in cell lysis. This condition is commonly called oxidative stress. It can be defined as a disturbance in the prooxidant-antioxidant balance in favour of the former leading to potential biomolecular damage caused by attack of reactive oxygen species (Halliwell, 2007). H_2O_2 generated extracellularly has been shown to diffuse readily across cell membranes into the cytoplasm (Imlay. 2008) where it is free to react with labile iron to form $^{\bullet}OH$ (Rxn 3). The length of time of exposure to a concentration of toxicant is an important factor in toxicological studies. In typical tank biooxidation and bioleaching processes average residence times are between 4 and 6 days. There is evidence to suggest that pyrite surfaces can generate ROS continually under certain conditions, particularly below pH 3, i.e. generation is not limited to initial contact with solution (Borda *et al*., 2001; Schoonen *et al*., 2010).

In this study two sulfide concentrates, pyrite and chalcopyrite, have been subjected to batch mechanical activation experiments for different time intervals using two laboratory mills: a planetary agate ball mill and a vibratory corundum microniser mill. Milled samples were analysed for changes to particle size distribution, surface area and X-ray diffraction line broadening. Sample reactivity in acidic solution was measured for by the generation of ROS. Finally, feed and milled samples were used in

batch bioleaching tests using a thermophilic culture to investigate the effects of mechanical activation. The objective of this study was to understand how the milled concentrates generated using the planetary and vibratory mills differed in macro and micro surface changes affecting reactivity, ROS generation, abiotic and biotic leach rates as well as the activity of microbial cultures used in flask (bio)leaching experiments.

2. Experimental

2.1 Materials and Microorganisms

Two sulfide concentrates were used: a non-gold containing pyrite (90.2% w/w) concentrate, produced for research purposes, and a copper containing chalcopyrite (65.9% w/w) concentrate. Samples were divided representatively using an auto-sampler into 20 g samples and stored in a vacuum desiccator prior to milling. Major minerals associated with the pyrite concentrate were szomolnokite (6.5% w/w) and quartz (1.5% w/w). The chalcopyrite concentrate contained talc (15.4% w/w), pyrite (11.7% w/w) covellite (5.0%w/w) and quartz (1.9% w/w). A non-specifically mixed thermophilic culture containing *Sulfolobus metallicus* (Nemati *et al*., 2000) and *Metallosphaera hakonensis* (H01-1) (laboratory isolate) was used for batch flask bioleaching tests on milled samples. Two stock cultures were adapted and maintained through sub-culturing in shake flasks on 1% (w/v) of each feed concentrate as the sole energy source and were used as inocula for the respective flask bioleaching tests.

Table 2. Dimensions and construction of laboratory mills and media

Mill	Chamber				Media				
	Inner Diameter [cm]	Height [cm]	Volume [cm^3]	Material	Diameter [cm]	Height [cm]	No.	Mass [g]	Material
Planetary	7.5	8.5	290	agate	2.1	sphere	25	10.7	agate
Vibratory	4.7	8.5	125	polypropylene	1.2	1.2	48	5.7	corundum

2.2 Milling experiments

Mechanical activation of sulfide concentrates was achieved via batch milling using two different laboratory mills: a planetary agate ball mill (Retsch) and a vibratory micronizer mill (McCrone). The application of the planetary ball mill is for general laboratory preparation of small samples whereas the vibratory micronising mill was specifically designed for use in powder X-ray diffraction (XRD) sample preparation. Table 2 shows the details of the milling chambers and grinding media of the two mills. Both mills were operated at maximum power for set periods of milling time and all milling experiments were performed wet under ambient conditions using 20 g concentrate (maximum vibratory mill charge load) and 20 g distilled water (50% w/w). Samples were collected from milling chambers by using a distilled water wash followed by an ethanol wash after which all the solids were filtered and air dried before being stored in a vacuum dessicator. Pyrite (Py) feed was milled in the planetary (P) mill for 5 (Py-P_5), 20 (Py-P_{20}) and 60 (Py-P_{60}) minutes respectively. Pyrite was milled in the vibratory (V) mill (Py-$V_{5,20,60}$) for the same time periods. Chalcopyrite (Ch) feed was milled in the planetary mill for 2.5

(Ch-$P_{2.5}$), 10 (Ch-P_{10}) and 40 (Ch-P_{40}) minutes. Chalcopyrite was milled in the vibratory mill for 2.5 (Ch-$V_{2.5}$), 10 (Ch-V_{10}) and 60 (Ch-V_{60}) minutes.

2.3 Analysis of particle characteristics

Volumetric particle size distributions were determined using laser diffraction (Malvern Mastersizer 2000). Uniformity, span and specific surface area were calculated to characterise these distributions:

(Eqn 1)

$$U=\frac{\sum X_i|d(0.5)-d_i|}{d(0.5)\sum X_i}$$

Uniformity (U) (Eqn 1) is the absolute deviation from the median diameter where d(0.5) is the median volume particle diameter and d_i and X_i are the mean diameter and sample volume percentage in class i respectively.

$$S=\frac{d(0.9)-d(0.1)}{d(0.5)} \quad \text{(Eqn 2)}$$

Span (S) (Eqn 2) is the distribution span where d(0.1,0.5,0.9) are particle sizes below which 10, 50 and 90% of the distribution volume lies respectively.

$$SSA=\frac{6\sum\frac{V_i}{d_i}}{\rho\sum V_i}=\frac{6}{\rho D[3,2]} \quad \text{(Eqn 3)}$$

Specific surface area (SSA) (Eqn 3) is the total geometric surface area divided by the totals weight of the particles, where V_i and d_i are the volume and mean diameter of particle class i and ρ is the sample density. D[3,2] is the Sauter mean. Sample surface area was measured using the 5-point N_2 adsorption Brunauer, Emmett and Teller (BET) method (Micromeritics TriStar) and density was measured using a helium pycnometer (Micromeritics AccuPyc 1330). Scanning electron micrographs were taken (Nova NanoSEM) and powder XRD spectra were obtained by using a Bruker D8 Advance powder diffractometer with Vantec detector and fixed divergence and receiving slits with Cu-Kα radiation. The phases were identified using Bruker Topas 4.1 software and the relative phase amounts (weight %) were estimated using the Rietveld method. Line broadening associated with intensive milling was analysed from the XRD spectral peaks of pyrite (200) and chalcopyrite (112) as full width half maximum (FWHM) 2θ/degree and degree of reference crystallinity (X_{ref}) calculated from fitted Gaussian distributions as well as calculating crystallite size (Topas 4.1) from fitted Cauchy-Lorentz distributions.

$$X_{ref}=\frac{U_0}{I_0}\cdot\frac{I_X}{U_X}\cdot 100\ (\%) \quad \text{(Eqn 4)}$$

The degree of crystallinity (X_{ref}) (Eqn 4) is calculated by comparison to a reference crystallinity, assumed to be 100%, usually of the head grade feed sample is calculated using the background intensity of first milled sample (U_0) and the mechanically activated sample (U_x) and the integral intensities of the diffraction peaks of the first milled (I_0) and mechanically activated sample (I_x) (Baláž *et al.*, 2000).

2.4 Detection of Reactive Oxygen Species

The fluorescence detection method for measuring reactive oxygen species (ROS), combination of hydrogen peroxide and hydroxyl radicals, in acidic solutions was adapted from Cohn *et al*. (2006). Small quantities of milled sample were incubated in 50 mL Erlenmeyer flasks for 24 h at 180 rpm in 30 mL of acidified (pH 1.6, H_2SO_4) basal salt medium (see below). All experiments were performed in triplicate and measured BET surface areas (m^2/g) of samples were used to normalise measured ROS values to a constant surface area loading (10 m^2/L). A ROS-dependent increase in APF fluorescence standard curve was generated by mixing 10 µM APF (3'-(*p*-Aminophenyl) Fluorescein, Invitrogen), 0.55 M potassium phosphate buffer at pH 5.40, 2.95 units/mL horseradish peroxidise (equivalent to 0.2 µM) (Serevac) and standard dilutions of H_2O_2 in a white, flat bottom 96 well fluorescence microtitre plate (BRAND pureGrade ref 781608). Sample measurements were performed in a similar way, replacing the H_2O_2 addition by 100 µL filtered (0.22 µm Milipore) and diluted samples to 100 µl of the rest of the reagent mixture. ROS induced fluorescence was measured using a FLUOstar OMEGA microtitre plate reader employing top optics only. After addition of ROS containing filtrate to the reaction mixture, samples were mixed in the microtitre plate reader for an additional 30 seconds using double orbital shaking (600 rpm). Temperature was held constant at 25℃ and fluorescence measurements were made using excitation/emission at 490/520 nm. Data generated are an average of 35 excitation/emission cycles per well using an orbital average at 4 mm diameter.

2.5 Thermophilic batch bioleaching experiments

Milled samples were bioleached in duplicate for up to 14 days at 2% (w/v) solids loading in 500 mL Erlenmeyer flasks at 300 mL total culture volume. The following basal salt medium was used: $(NH_4)_2SO_4$ (1.30 g/L), KH_2PO_4 (0.28 g/L), $MgSO_4.7H_2O$ (0.25 g/L) and $CaCl_2.2H_2O$ (0.07 g/L), supplemented with 0.20 g/L yeast extract and 0.15 g/L tetrathionate. The pH was adjusted to 1.6 with H_2SO_4 and 0.10 and 1.67 g/L of Fe^{3+} iron was added to pyrite and chalcopyrite flasks respectively at the beginning of the experiment. Flasks were inoculated with $1X10^7$ cells/mL adapted stock cultures and incubated at 65℃ on an orbital shaking incubat or (180 rpm). Samples were taken daily and the following measured: Redox potential (Crison ELP 21); pH (Metrohm 704); total and Fe^{2+} iron measured colorimetrically using 1-10 phenanthroline method (Valencia and Acevedo, 2009); planktonic cell counts (Thoma counting chamber, Olympus BX-40 microscope); soluble copper (chalcopyrite flasks) using atomic absorption spectroscopy were measured every other day. Fluorescent microscopy was used to assess total cells associated with sulfide particles by staining samples with non-specific nucleic acid molecular probe SYBR® Gold (Invitrogen) according to Bryan *et*

al. (in preparation). Fluorescent microscopy was used to confirm that abiotic control experiments were free of contamination. The loss of water due to evaporation was compensated for by adding distilled water gravimetrically.

2.6 Batch data analyses

Initial iron and copper solubilisation rates ($Q_{Fe/Cu}$) were calculated from pyrite and chalcopyrite solubilisation curves as the slope of the straight lines drawn through time points 0 and 5 days, using linear interpolation to calculate concentration data for day 5. Extent of iron and copper leached ($\varepsilon_{Fe/Cu}$) was calculated from the maximum soluble concentration measured within 14 days. Redox potential lag times were calculated as the time point at which a 5% increase of the total measured redox range occurred from the lowest measured value.

3. Results and discussion

3.1 Particle characterisation following sulfide concentrate milling experiments

Analysis of the head sulfide feeds (Table 2) showed that the chalcopyrite feed was finer than the pyrite feed with sample median (D_{50}) of 105.6 µm and 10% of the particle volume (D_{10}) below 14.2 µm whereas the same pyrite feed values are 165.2 µm and 66.5 µm respectively. The two mills chosen for this study operate by different particle breakage mechanisms (Pourghahramani and Forssberg, 2007) as can be seen by the product particle size distributions (Fig. 1) of the milled samples. Particle size distributions were analysed on a volume basis. Both pyrite and chalcopyrite milled samples showed the same trends across mill type. The vibratory mill produced narrower and more uniform particle size distributions with increased milling time (Table 3), as indicated with smaller distribution span values and uniformity measurements. This is an indication that the particle breakage mechanism of the vibratory mill is dominated by attrition breakage (Ye *et al*., 2010). The planetary mill produced broader and less uniform distributions with increased milling time, indicative of a particle compression or fracture breakage dominated mechanism.

The production of fine (<10 µm) particles with increased milling time is indicated by the decreasing D_{50} values below 10 µm of samples milled for 10 min or more, with the exception of the Ch-V_{10} sample (D_{50} = 13 µm). The generation of ultrafine particles (<1 µm) can be seen in all milled particle size distributions of both pyrite and chalcopyrite, it is more acute with milled chalcopyrite samples due to the finer feed. The ultrafine content of Ch-P_{40} and Ch-P_{60} samples is 24.5 and 16.9% respectively on a volume basis. The distributions of milled chalcopyrite are observed to be more bimodal with increased milling time and may possibly suggest that there is an increased contribution to ultrafine particle generation caused by a shift in particle breakage mechanism nearing the respective grind limits of the two mills (Yue and Klein, 2005). This cannot be confirmed without proper examination of particle breakage within the two mills, a challenge with particles below 5 µm.

The measurement of surface area is important when studying the reactivity of sulfide particles. Mechanically activated sulfides react on exposure to air at ambient conditions to form of secondary

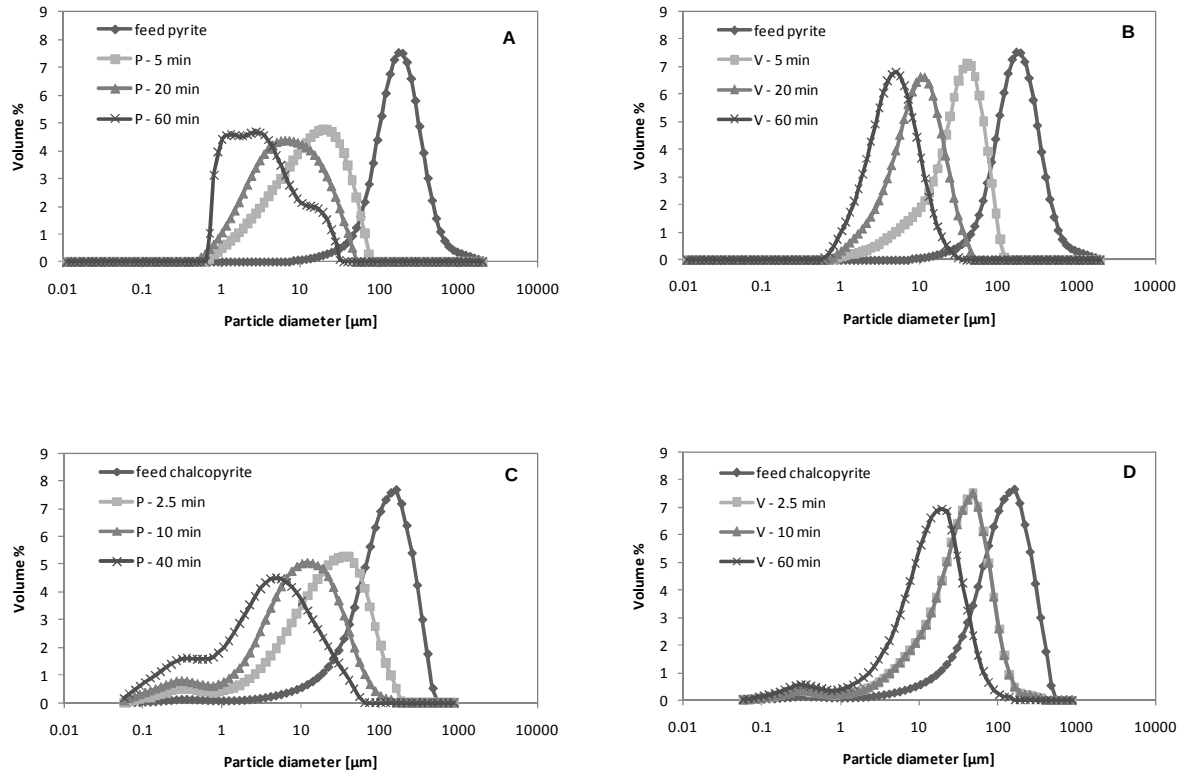

Figure 1. Particle size distributions of planetary (A,C) and vibratory (B,D) milled pyrite and chalcopyrite samples. Pyrite (A,B) and chalcopyrite (C,D) samples milled with planetary (P) and vibratory (V) mills as a function of milling time.

layers that coat particles over time. A study by Hu *et al.* (2007) showed oxidation of a pyrite surface to solid iron sulfate products such as $FeSO_4.H_2O$, $Fe_3(SO_4)_4.14H_2O$ and $Fe_2(SO_4)_3.H_2O$. To minimise surface oxidation subsequent to milling, all surface area measurements were performed within 1 week of milling and samples were stored in a vacuum dessicator. Figures 2 and 3 show scanning electron micrographs of feed and milled pyrite and chalcopyrite samples. The presence of fine particles and amorphous surface oxidation products was observed in the chalcopyrite feed using SEM-Electron Dispersion Spectroscopy analysis (data not shown) to identify oxygen containing phases. Surface oxidation products were also particularly prevalent in intensively milled 40 and 60 min pyrite and 60 min chalcopyrite samples. Sample surface area was measured using N_2 gas adsorption according to the Brunauer, Emmett and Teller (BET) method determined to be the most accurate and consistent measure of sample surface area. This was compared to the Specific Surface Area (SSA), determined from volumetric particle size distribution. Attempts were made to quantify surface area using image analysis of images acquired by light microscopy (data not shown). SSA values are a calculated measure of the sample geometric surface area assuming spherical particles. In Table 3 the BET and SSA data are given for all samples. Comparing SSA and BET values for both mills and sulfide samples shows that SSA values were significantly smaller and underestimate sample surface area due, in part, to the non-spherical particles of irregular shapes seen in Figs. 2 and 3. BET surface area

includes all areas of irregular shaped particles including inner surface, such as cracks and pores. The rate of new surface area generated per mass of milled sample over milling time was much larger for

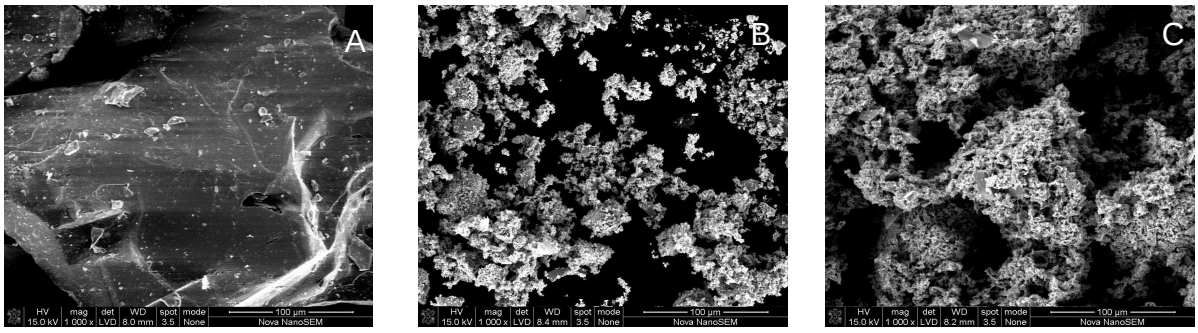

Figure 2. SEM of pyrite samples. Feed (A), 60 min planetary (B) and 60 min vibratory (C) milled samples. Samples prepared with the same washing and filtering procedure prior to images being taken.

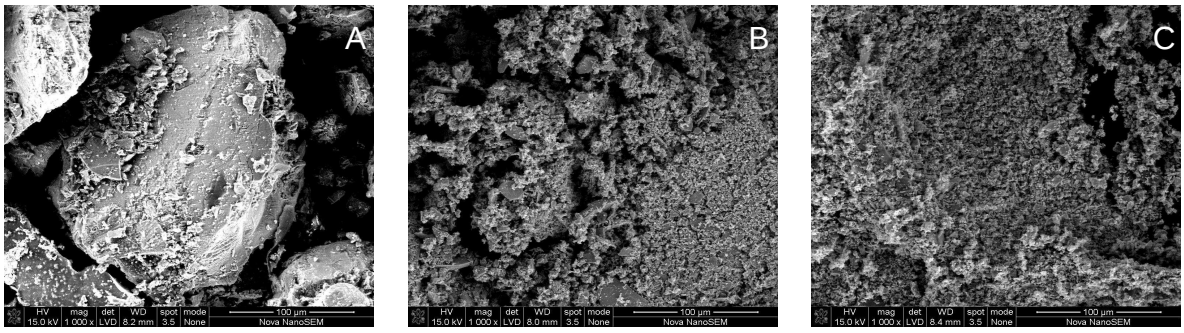

Figure 3. SEM of chalcopyrite samples. Feed (A), 40 min planetary (B) and 60 min vibratory (C) milled samples. Samples prepared with the same washing and filtering procedure prior to images being taken.

the planetary mill than the vibratory mill. There was a 69.6 and 2.4 fold increase in surface area for pyrite and chalcopyrite feeds respectively at maximum milling times (40 and 60 min). Use of the vibratory mill increased feed pyrite and chalcopyrite surface area by 22.4 and 1.76 fold relative to the feed at maximum milling time of 60 min. The Sauter mean value is an indication of the approximated surface area distribution within a particle size distribution and is a measure of where 50% of the specific surface area is above and below a certain particle size. Sauter mean values were seen to decrease below 10 µm in all milled samples with increased milling time with the exception of vibratory 5min milled pyrite. This highlights the large contribution that fine and ultrafine particles have to the overall sample surface area.

Sample densities were measured (Table 3) and observed to decrease with increasing milling time for most samples. Correlation between sample surface area and density was observed for both mills and

sulfide samples. Decreasing density may be caused by the presence of iron sulfate oxidation products which have smaller densities (1.9 – 2.8 g/cm^3) than pure pyrite (±4.9 g/cm^3) and chalcopyrite (±4.1 g/cm^3). Other sulfide and silicate mineral phases measured (data not shown) in head pyrite (10%) and chalcopyrite (34%) samples were shown to be constant throughout all milled samples. The initial increase in chalcopyrite sample density after brief milling with both mills was attributed to the

head chalcopyrite sample being heavily oxidised prior to milling (Fig. 3) and most of the oxidation mass being lost by milling and washing in sample preparation.

Table 3. Sulfide feed and milled sample product size distribution, surface area and density analyses

Mill	Milling time [min]	Particle size distribution[a]					Sauter[b] mean [µm]	SSA[c] [m^2/g]	BET[d] [m^2/g]	Density [g/cm^3]
		D_{10} [µm]	D_{50} [µm]	D_{90} [µm]	Span	Uniformity				
Pyrite										
	feed	66.49	165.18	374.73	1.87	0.634	118.495	0.010	0.105	4.953 (± 0.005)
Planetary	5	2.67	12.66	37.69	2.77	0.850	6.505	0.190	1.265	4.863 (± 0.008)
	20	1.66	6.31	21.84	3.20	0.973	3.870	0.326	3.610	4.758 (± 0.012)
	60	0.97	2.81	12.70	4.17	1.190	2.153	0.602	7.284	4.632 (± 0.007)
Vibratory	5	7.09	30.31	64.19	1.88	0.575	14.950	0.082	0.438	4.917 (± 0.006)
	20	2.85	8.95	21.00	2.03	0.628	5.975	0.207	1.310	4.854 (± 0.006)
	60	1.66	4.39	10.54	2.02	0.637	3.327	0.374	2.345	4.821 (± 0.005)
Chalcopyrite										
	feed	14.20	101.57	291.41	2.73	0.846	8.52	0.174	3.452	4.055 (± 0.003)
Planetary	2.5	2.33	19.94	69.17	3.35	1.047	2.89	0.512	4.624	4.057 (± 0.004)
	10	0.85	8.76	33.20	3.69	1.171	1.6	0.925	6.250	4.052 (± 0.007)
	40	0.28	3.46	16.81	4.78	1.484	0.83	1.793	8.234	4.032 (± 0.006)
Vibratory	2.5	5.08	30.56	76.93	2.35	0.764	4.71	0.314	4.251	4.063 (± 0.002)
	10	2.22	13.00	35.20	2.54	0.811	2.7	0.547	4.494	4.063 (± 0.004)
	60	0.41	4.11	11.75	2.76	0.896	1.11	1.340	6.071	4.035 (± 0.004)

[a] Particle size distribution data calculated from volume distribution measured by laser diffraction

[b] Sauter mean is a measure of surface area mean diameter calculated from volume distribution

[c] Specific surface area is a geometric measure of surface area assuming sphereical particles calculated from volume distribution

[d] BET standard error calculated to be less than 10%

XRD spectral line profile analysis can be used to determine crystal lattice microstrain and crystallite size calculated from reduction of peak height and line broadening (Pourghahramani and Forssberg, 2006). Figure 4 shows the powder XRD spectra for pyrite and chalcopyrite with the respective phase peaks highlighted. Line broadening associated with pyrite 200 and chalcopyrite 112 peaks was investigated by fitting Gaussian distributions to the experimental data and calculating full width half maximum (FWHM) values (Table 4) of the fitted distributions. Chalcopyrite diffraction peak 112 has been used previously for line profile analysis to study intensive dry-milling of chalcopyrite in a planetary mill (Bafghi *et al*., 2009). A positive correlation between milling time and FWHM values was

observed for all planetary milled samples whereas no clear trend was observed for vibratory milled samples with calculated values remaining constant as a function of milling time. Mean crystallite sizes of the respective pyrite and chalcopyrite crystallites within the milled samples were estimated from fitted Cauchy-Lorentz distributions, using Topas 4.1 software, and are an indicator of the mean size of pyrite and chalcopyrite crystallites present within the milled sample particles as a distribution of crystallite sizes. A decrease of crystallite size with increased milling time was observed for all

samples with the exception of the pyrite vibratory milled samples varying slightly around 465 nm. A significant reduction of crystallite size occurred for pyrite planetary milled samples from 738 nm at 5 min of milling time to 157.2 nm at 60 min.

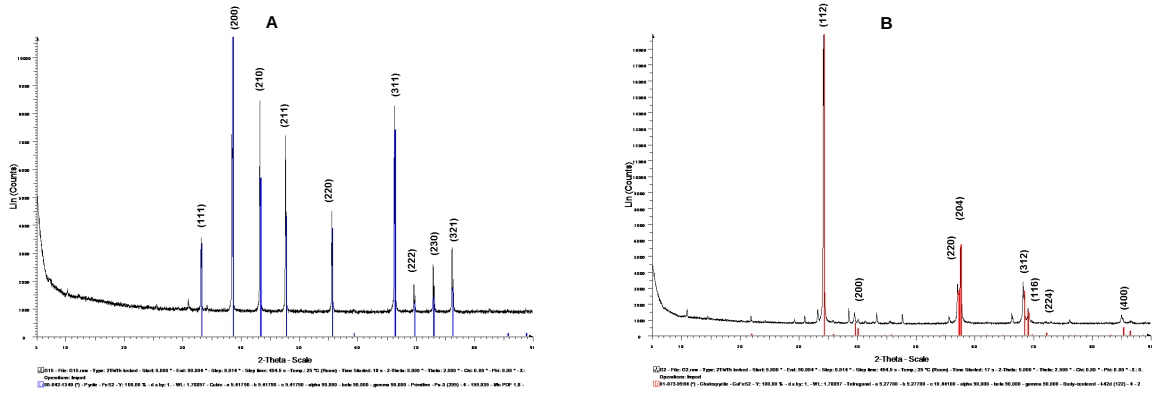

Figure 4. Pyrite and chalcopyrite sample XRD spectra. Pyrite (A) peak 200 and chalcopyrite (A) peak 112 analysed for line broadening at different milling times.

A measure of crystallinity can be calculated from line profile analysis using a reference sample, usually a head sample or a sample as received from the supplier (Baláž *et al.*, 2000). The crystallinity of the reference is assumed to be 100% allowing for the degree of crystallinity (X_{ref}) to be calculated from subsequently milled samples. However in this study, both pyrite and chalcopyrite feed sample particle sizes were too large to yield accurate XRD data. Therefore the degree of sample crystallinity was determined relative to the first milled sulfide sample of each mill, hence calculated values are an indication of variation in the degree of crystallinity with increased milling time within subsets of data. Comparison of milled sample values (Table 4) indicated a greater extent of crystal structure deformation within milled chalcopyrite samples compared to pyrite milled samples which showed negligible differences. Loss of crystallinity occurred at a faster rate for planetary mill than the vibratory mill when comparing chalcopyrite samples. Similar results were observed for milling experiments conducted with hematite in a planetary mill compared to a vibratory mill (Pourghahramani and Forssberg, 2007).

3.2 Generation of ROS from mechanically activated sulfides

Schoonen (2010) and co-workers investigated ROS generation and decomposition from pyrite slurries and noted that pyrite surface oxidation products such as ferric oxides and hydroxides were sites of hydrogen peroxide decomposition. These sites are believed to be stable at pH above 3 and persist on the surface preventing hydrogen peroxide from accumulating in solution. Below pH 3, the pyrite surface is expected to be free of ferric oxidation sites thus allowing hydrogen peroxide to accumulate in solution. Therefore to investigate the reactivity of milled sulfide samples in solution, solution conditions relevant to biohydrometallurgy were maintained. ROS generation was measured at 24 h following incubation of a measured mass of sample in pH 1.6 basal salt medium at 65 ℃. Filtered samples were then incubated with peroxidase enzyme and fluorescent probe using a very strong

potassium phosphate buffer, free of organic constituents that would react with hydroxyl radicals, to raise the pH from 1.6 to 5.4.

Table 4. Comparison of FWHM values, crystallite sizes and reference crystallintity of milled samples

Mill	Pyrite				Chalcopyrite			
	Milling time [min]	FWHM [2θ/degree]	Crystallite size [nm]	X_{ref} [%]	Milling time [min]	FWHM [2θ/degree]	Crystallite size [nm]	X_{ref} [%]
Planetary	5	0.168	738.4	100.0	2.5	0.196	140.1	100.0
	20	0.182	395.6	99.7	10	0.252	73.8	71.3
	60	0.252	157.2	99.4	40	0.392	45.0	53.5
Vibratory	5	0.182	499.0	100.0	2.5	0.210	161.8	100.0
	20	0.154	429.7	99.4	10	0.182	153.9	86.3
	60	0.168	465.9	99.2	60	0.280	64.1	67.6

In biohydrometallurgical treatment of mechanically activated concentrates, it is important to monitor sulfide reactivity with respect to the generation of toxic reactive oxygen species which have the potential to inhibit acid and Fe^{3+} iron generation from the microbial population via the oxidative stress response. An alternative explanation for the observed decreased performance of intensively milled samples is the lack of “attachable” surface due to the fine size of the particles, most of which are the actual size or smaller than individual microbial cell size (±1 µm). Gautier *et al.* (2008) found that attachment of *Sulfolobus metallicus* cells to chalcopyrite was important for effective bioleaching to occur whereas growth was restricted when inoculated cells were prevented from approaching and attaching to chalcopyrite. The formation of agglomerates from fine particles (Baláž, 2003) may also contribute towards the loss of mineral surface area availability and cause a decrease in performance. However, both these explanations only describe conditions of inhibited microbial performance and not the complete absence as was observed in this study and other similar studies, suggesting that the oxidative stress effect caused by the generation of toxic ROS from mechanically activated sulfides does have a significant effect that may work simultaneously with other factors to cause culture death.

Fig. 5 depicts the ROS generation results. All values were normalised to 10 m^2/L surface area loading for comparison. A significant difference between pyrite and chalcopyrite ROS generation was observed. Pyrite samples produced significantly more ROS compared to chalcopyrite. Also, the planetary milled samples generated more ROS than the vibratory milled samples, with 6.27 and 4.36 fold increases from unmilled pyrite and chalcopyrite feeds respectively at maximum milling times in the planetary mill. Measured increases in ROS for vibratory milled samples were 1.39 and 3.39 fold for

pyrite and chalcopyrite relative to unmilled feeds. The ROS values correspond to a combined measurement of both hydrogen peroxide and hydroxyl radicals at 24 h of sample incubation in acid (pH 1.6). However, the dominant reactive species has been measured as hydrogen peroxide (data not shown) which is known to be more stable under acidic conditions (Schoonen *et al*., 2010). Another mechanism for ROS generation has been identified from sulfide mineral release of metal ions

into solution. Fe^{2+} iron released from surface oxidation products present on mechanically activated samples is available for reaction with dissolved oxygen in the Haber-Weiss reactions (reaction 1 and 2) which can also occur on the surface. Although ROS measurements were normalised to surface

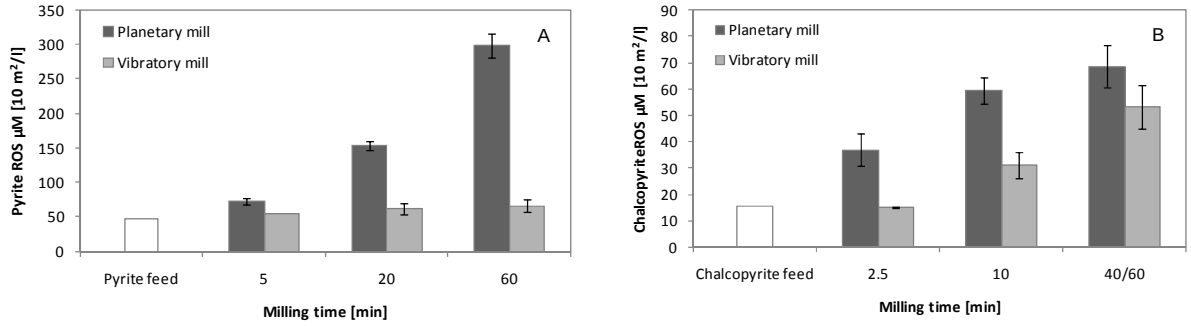

Figure 5. Surface area loading normalised ROS generation following 24 h incubation. Pyrite (A) and chalcopyrite (B) feed and milled samples incubated in pH 1.6 basal salt medium at 65 ℃ for 24 h. Average ROS values normalised to 10 m^2/L surface area loading calculated from BET and standard error presented.

area loading, it cannot be assumed that surface oxidation was uniform on particles. Therefore it cannot be assumed that there was an equivalent amount of Fe^{2+} iron solubilised per unit of milled surface area and it is possible that the contribution to ROS generation from solubilised iron was more significant with more intensively milled samples. In the absence of the biological oxidation of Fe^{2+}, the majority of the soluble iron in the presence of pyrite and chalcopyrite remained as Fe^{2+} iron due to the fact that any Fe^{3+} iron formed via abiotic oxidation would be reduced at the sulfide surface.

3.3 Thermophilic bioleaching flask experiments

Biotic (bioleaching) and abiotic leaching data are summarised in Table 5 and a subset of the raw data (feed and planetary milled chalcopyrite samples) shown in Fig. 6. To examine the contribution that microbial action had on bioleaching experiments, it was necessary to perform abiotic control experiments under the same starting conditions. The starting Fe^{3+} concentration was the only condition changed between pyrite (0.10 g/L) and chalcopyrite (1.67 g/L) flask experiments. In Fig. 6 D abiotic copper solubilisation is presented as a function of leaching time from the feed and planetary ball milled chalcopyrite samples. The hydrometallurgical benefit of mechanically activating chalcopyrite via milling prior to leaching can been seen in increased initial leach rates (Q_{Cu}) from 0.062 g Cu/L/d for unmilled feed to 0.533 g Cu/L/d for 40 min milled chalcopyrite. The extent to which copper is leached (ε_{Cu}) was also greatly improved with only 9.6% being leached from unmilled feed compared with 70.3% for 40 min planetary milled sample at 14 days. Redox potential and Fe^{2+} iron measurements showed that after the initial consumption of Fe^{3+} iron, the abiotic leach flasks were dominated by Fe^{2+} iron (data not shown). Other leaching experiments conducted on milled chalcopyrite in ferric sulfate medium (Baláž, 2003) concluded that in the leaching of mechanically activated samples the first step was the dissolution of copper from surface oxidation layers formed during milling and then the leaching of copper from sites of non-stoichiometric chalcopyrite ($CuFeS_{2-x}$)

which are a result of surface defects and bulk particle deformation. The improvement in leach rates was therefore more closely related to a combined measure of sample surface area and degree of crystallinity, measured by analysis of XRD spectra, rather than milling time alone. A similar result is

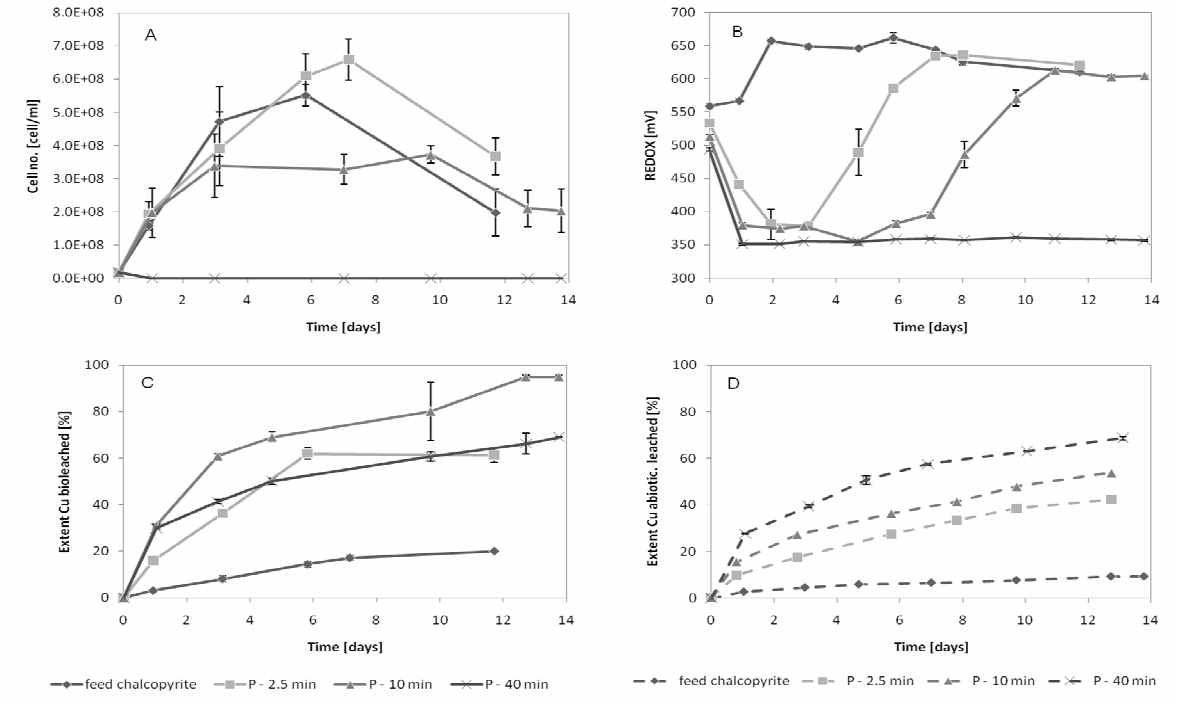

Figure 6. Chalcopyrite flask bioleach and abiotic leach raw data of feed and planetary agate ball milled 2.5, 10 and 40 min samples 2% (w/w). Planktonic cell counts (A), redox measurements (B), extent of copper bioleached (C) and copper leached abiotically (dashed lines) (D). Mean duplicate flask data presented with standard deviation error bars.

observed here with both chalcopyrite and pyrite samples. Improved leach rates were correlated more closely to increased surface area loading (SAL) in solution (Fig. 7) at 2% w/v pulp density for the start of the experiment than milling time. The lower pyrite (Fig. 7A) leach rates and extents at higher SAL (>50 m^2/L) may result from lower Fe^{3+} in solution, due to lower starting Fe^{3+} concentration compared with chalcopyrite (Fig. 7B) experiments.

The bioleaching tests showed that there was large improvement of inoculated samples, where microbial activity was observed, in terms of initial rates and extents for pyrite and chalcopyrite. Ch-$P_{2.5}$ and Ch-P_{10} bioleached samples (Fig. 6 A-C) showed an increase of the initial bioleach rate compared to the unmilled feed from 0.131 to 0.567 and 0.733 mg Cu/L/d and 21.5 to 61.1 and 97.6% for the extent of copper leached for 0, 2.5 and 10 min milling respectively at 14 days (Table 5). A maximum extent of iron bioleached from planetary milled samples was observed at 83.3% for Py-P_5 compared to only 11.0% for the pyrite feed. Only soluble total iron was measured in these experiments and the contribution from precipitated iron was ignored. Vibratory milled pyrite, Py-$V_{20,60}$, and chalcopyrite, Ch-V_{60}, yielded greater bioleaching rates and extents compared with planetary milled samples at increased milling times.

Comparing leach rates of milled bioleached samples as a function of SAL (Fig. 7) showed two different responses for both pyrite and chalcopyrite. Improved leaching rates were observed with increasing

SAL up to a maximum point, specific to each sulfide, followed by a decrease in leach rates with further increases in SAL at 2% w/v pulp density. Maximum leach rates for mechanically activated pyrite and chalcopyrite samples were observed at approximately 26 and 125 m^2/L respectively. Increases in SAL

Table 5. Summarised thermophilic bioleaching flask data

Mill	Milling time [min]	SAL [m^2/L]	Abiotic		Biotic			
			$Q_{x=Fe/Cu}$ [g x/L/d][a]	$\square_{Fe/Cu}$ [%][b]	$Q_{x=Fe/Cu}$ [g x/L/d]	$\square_{Fe/Cu}$ [%]	Max. Cell no. [cell/ml]	Redox lag [d]
Pyrite								
	feed	2.1	0.025	3.5	0.174	11.0	5.89E+08	0.54
Planetary	5	25.3	0.171	26.6	0.598	83.3	3.61E+08	2.14
	20	72.2	0.296	46.1	0.291	41.7	1.00E+07	na
	60	145.7	0.405	61.2	0.453	57.6	1.00E+07	na
Vibratory	5	8.8	0.057	27.0	0.526	84.6	4.73E+08	2.04
	20	26.2	0.168	29.2	0.646	77.8	3.03E+08	2.19
	60	46.9	0.262	45.0	0.552	78.5	2.52E+08	2.01
Chalcopyrite								
	feed	69.0	0.062	9.6	0.131	21.5	5.52E+08	0.60
Planetary	2.5	92.5	0.258	45.1	0.567	61.1	6.59E+08	3.31
	10	125.0	0.353	56.4	0.733	97.6	3.72E+08	5.27
	40	164.7	0.533	70.3	0.517	69.3	1.00E+07	na
Vibratory	2.5	85.0	0.140	42.6	0.369	51.3	6.56E+08	1.37
	10	89.9	0.279	48.9	0.566	81.7	4.14E+08	3.50
	60	121.4	0.350	67.5	0.755	100.0	3.52E+08	7.00

[a] $Q_{x=Fe/Cu}$ is the initial solubilisation rate measured after 5 days of bio/leaching in g/L/d of either iron or copper

[b] $\square_{Fe/Cu}$ is the extent of iron or copper bio/leached in weight percentage from pyrite or chalcopyrite after 14 days

beyond these maxima resulted in decreased leach rates, most notably for Py-$P_{20,60}$ and Ch-P_{40} milled samples. These planetary milled samples yielded leach rates similar to the equivalent abiotic leached samples indicating a lack of microbial associated bioleaching activity. There was evidence of microbial activity in chalcopyrite feed and both Ch-$P_{2.5,10}$ (Fig. 6A) samples with maximum planktonic cell concentrations of 5.52, 6.59 and 3.72 X 10^8 cell/mL respectively. The lag period preceding increase in redox potential (Fig. 6B) differed considerably at 0.60, 3.31 and 5.27 days for 0, 2.5 and 10 min respectively. The three flasks proceeded to reach high redox values (>600 mV). Passivation of chalcopyrite at high redox potentials owing to the formation of Fe^{3+} precipitates on particle surfaces is a well studied phenomenon.

A lack of microbial activity was observed for Ch-P_{40}. The planktonic cell concentration decreased from starting inoculum cell concentration of 1.0 X 10^7 to 3.91 X 10^5 cell/mL at 1 day. The planktonic cell

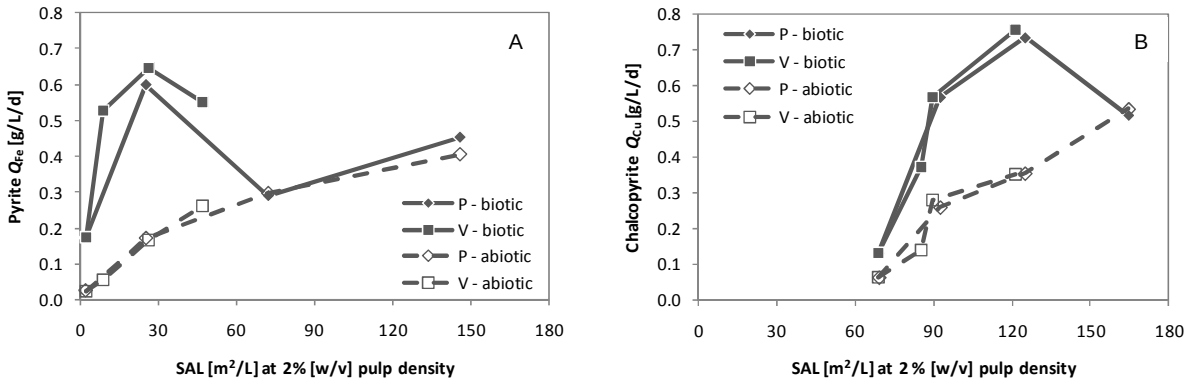

Figure 7. Biotic and abiotic initial solubilisation rates as a function of surface area loading at the beginning of the experiment. Pyrite (A) and chalcopyrite (B) feed and milled samples. Surface area loading calculated at from BET values at 2% w/v pulp density.

concentration was below the detection limit (3.0 X 10^5 cells/ml) at 3 days and remained below the detection limit thereafter. Fluorescent microscopy (Fig. 8) was used to monitor semi-quantitatively the total cell concentration, planktonic and particle associated, and was found to correspond with planktonic cell counts. Fluorescent cells were observed (Fig. 8A) from slurry samples taken immediately after inoculation whereas no fluorescent cells were observed to be associated with Ch-P_{40} particles after 2 days from inoculation (Fig. 8B). A similar trend was observed for Py-$P_{20,60}$ samples corresponding with observations made on analysis of leach rates. It is assumed that cell lysis resulted in no detectable cells. The redox potential profile (Fig. 6B) for Ch-P_{40} showed no increase in redox potential (±350 mV) after the initial consumption of available Fe^{3+} iron. Fe^{2+} measurements confirmed that that the majority of the iron in solution was Fe^{2+}. The pH values showed that acid was consumed with an increase of pH from 1.6 to approximately 2.0 after which no measured decrease in pH was observed (data not shown). A decrease in pH below 1.6 was measured for feed and Ch-$P_{2.5,10}$ samples. A similar trend of responses was observed for Py-$P_{20,60}$ samples. A lack of microbial activity was observed with respect to planktonic cell counts being below the detection limit and low redox measurements (<400 mV). No fluorescent cells were observed using fluorescent microscopy. Microbial activity was observed in all vibratory milled samples. Increased performance was observed for vibratory milled bioleached samples compared to unmilled feeds. Vibratory milled pyrite at 5, 20 and 60 min showed that the corresponding initial bioleach rates and extents varied only by 20 and 10% respectively and were on average 3.7 and 7.0 fold higher than the unmilled feed bioleach data. The delays preceding the increase in redox potential were similar (±2 days) and the maximum planktonic cell counts were all above 2.5 X 10^8 cells/mL, with a slight decrease observed with increased milling time. Greater variation in bioleach performance was found for chalcopyrite following vibratory milling compared to milled pyrite over the same milling time. Compared to unmilled

chalcopyrite, there was 4.6 and 5.6 fold increase in Q_{Cu} and ε_{Cu} values for 60 min vibratory milled and 100% of the copper was bioleached at 9.7 days. The lag times preceding increase in redox potential

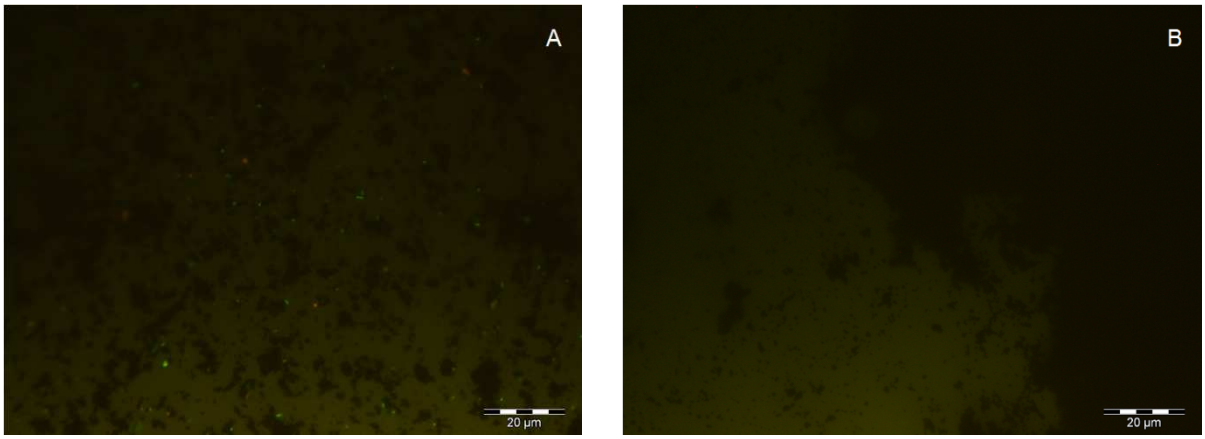

Figure 8. Fluorescent micrographs of stained samples taken from planetary agate ball milled 40 min bioleach flask. Sample taken at the start of experiment inoculated with 1 X 10^7 cells/mL (A). Sample taken at day 3 (B).

were 1.37, 3.50 and 7.0 days for 2.5, 10 and 60 min milling respectively. Maximum planktonic cell counts were all above 3.52 X 10^8 cells/mL, with a slight decrease with increased milling time.

Previous studies conducted by Baláž and co-workers showed that inhibition of bioleaching performance of mesophile *Acidithiobacillus ferrooxidans* occurred in the presence of finely milled pyrite and chalcopyrite (Baláž *et al*., 1996; Baláž *et al*., 1991) at 60 and 30 min of milling in a planetary mill respectively. Critical points in sample surface area and degree of crystallinity were found to correspond to bioleaching activity. Below a certain measured surface area and above a certain degree of crystallinity, improved bioleaching performance was observed with increased milling time, measured by increases in iron and sulfate solubilisation rates. Above this surface area and below a certain degree of crystallinity, the opposite microbial bioleaching response was observed.

Hydrogen peroxide formed at defect sites from dissolved oxygen and water on pyrite surface (Borda *et al*., 2003) has been shown to be a reacting intermediate in the abiotic auto-oxidation of pyrite (Schoonen *et al*., 2010). Experiments with a hydrogen peroxide specific degrading enzyme (catalase) showed that auto-oxidation could be significantly inhibited with enzyme incubation. Addition of hydrogen peroxide to pyrite and chalcopyrite sulfuric acid slurries has been modelled (Dimitrijevic *et al*., 1996; Antonijevic *et al*., 2004) with respect to leaching kinetics at different temperatures and particle size distributions and has shown that both pyrite and chalcopyrite leach at a first-order reaction rate with respect to hydrogen peroxide concentration and leach rates are also significantly increased at high temperatures and smaller particle sizes. Although the ROS concentrations (mostly hydrogen peroxide) measured from milled sulfides in this study are 2 to 3 orders of magnitude smaller than the hydrogen peroxide concentrations used in the previously mentioned studies, approximated at the same particle loading conditions, it is feasible that hydrogen peroxide formed on contact with

solution and for the duration of the flask experiments contributed towards the dissolution of iron and copper from pyrite and chalcopyrite.

Putting these results into context with ROS generation data it is possible to approximate the potential ROS concentration at the start of the flask experiments. Not only did samples which have been intensively milled have a larger SAL values, the ROS generation experiments also showed that intensively milled surfaces generated more ROS than briefly milled samples. These conditions lead to the accumulation of toxic hydrogen peroxide and hydroxyl radicals in solution and may reach cell damaging concentrations or even result in cell death if the cell is unable to respond and adapt to the oxidative stress conditions. Other thermophilic bioleaching studies, using classified samples prepared via wet sieving or gravity separation, conducted with *Sulfolobus metallicus* to investigate the microbial response to increased pyrite surface area loading, either by decreasing particle size or increasing pulp density or both, have shown negative effects such as decreased leach rates or even the complete lack of microbial activity (Nemati *et al*., 2000; Valencia and Acevedo, 2009), even with culture adaptation. Different methods of surface area analysis makes direct comparison to the present study difficult; however, the same trend can be seen where for small increases in surface area there is an increase in bioleaching performance while at high SAL conditions inhibition and sometimes a complete lack of microbial activity was observed.

4. Conclusions

The use of thermophiles in treating sulfide concentrates has thus far shown limited applicability in niche operations, such as BioCop, primarily due to the increased sensitivity of thermophiles towards high solids loading compared to other mesophilic species. However, the potential for using thermophiles in leaching copper from chalcopyrite is driven by the elevated temperatures needed for faster leach rates and better extraction efficiencies compared to bioleaching chalcopyrite at mesophilic temperatures.

The majority of bioleaching studies investigating microbial response to different sulfide particle conditions have varied the pulp density or particle size distribution with sample preparation mostly via wet screening classification. The challenge with this method of sample preparation is that the mineralogical composition is unconserved among subsequent samples and can vary greatly depending on the extent of heterogeneity of the head sample, complicating the analyses of bioleaching experimental results. Wet milling largely conserves the mineralogical composition provided that proper sampling is conducted prior to milling. Also the mechanism whereby particle reduction occurs industrially for the purpose of bioleaching is through re-grinding and not selective classification prior to tank feeding, therefore understanding sulfide mechanochemistry and the extent to which sulfide mineral reactivity is affected and affects the micro-organisms implicated in thermophilic bioleaching is important for improving thermophilic technologies.

On exposure of sulfide mineral concentrates, in this study pyrite and chalcopyrite concentrates, to wet milling, reactivity has been shown to change with respect to contacting particle solids with acidic solution. Increased surface area and disordering of the crystal structure were demonstrated and were beneficial in terms of improving mineral reactivity and leaching performance. Limited passivation of chalcopyrite particles may also be achieved through selected use of mechanical activation. Increased reactivity on increased milling correlated to the generation of reactive oxygen species (ROS) and increased specific surface area (SSA). This trend was more dominant for the planetary mill than the vibratory mill, indicating the importance of mill selection. Both abiotic and biotic leach rates were improved by milling of the concentrates in either mill. Biotic rates exceeded abiotic rates by two to three fold under most conditions. On extensive milling using the planetary mill, inhibition of biotic leaching was demonstrated. This was confirmed by an increasing lag time, negative growth rate and decrease or absence of microbial cells under these conditions. Microbial inhibition or lysis was attributed to oxidative stress in the presence of ROS.

The gains of mechanical activation of concentrates prior to (bio)leaching must be weighed against the cost of re-grinding sulfides and the ability to treat post-leached solid waste streams with different solid-liquid separation characteristics. The mechanical activation of sulfide rich concentrates and tailings is an important process step for efficient biohydrometallurgical processing, particularly of recalcitrant sulfides such as chalcopyrite. The hydrometallurgical benefits of mechanical activation combined with the ability of bioleaching microorganisms to adapt, within limits, to changing solids conditions may widen the applicability of bioleaching technologies to different and more refractory metal containing sulfide ore bodies.

Acknowledgements

The authors gratefully acknowledge the financial support from the National Research Foundation (NRF), the Department of Science and Technology, South Africa through the SARChI Research Chair in Bioprocess Engineering. The authors would like to acknowledge the technical support of Miranda Waldron of the Electron Microscope Unit, University of Cape Town.

References

Antonijević M.M., Janković Z.D., Dimitrijević M.D., Kinetics of chalcopyrite dissolution by hydrogen peroxide in sulphuric acid. Hydrometallurgy, 2004, 71, 329–334.

Bafghi M.S., Emamia A.H., Khakib J.V., Zakeri A., Development of a mathematical expression for the variation of amorphization phenomenon during intensive milling of minerals. International Journal of Mineral Processing, 2009, 93 (2), 149-154.

Baláž P., Kupka D., Bastl Z., Achimovicová M., Combined chemical and bacterial leaching of ultrafine ground chalcopyrite. Hydrometallurgy, 1996, 42, 237-244.

Baláž P., Mechanical activation in hydrometallurgy. International Journal of Mineral Processing, 2003, 9/29, 72 (1-4), 341-54.

Baláž P., Špaldon F., Luptáková A., Paholič G., Bastl Z., Havlík T., *et al*. Feasibility of a *Thiobacillus ferrooxidans* bacterial leaching of a chemically preleached chalcopyrite. International Journal of Mineral Processing, 1991, 32 (1-2), 133-146.

Baláž P, Takacs L, Luxová M, Godočíková E, Ficeriová J. Mechanochemical processing of sulphidic minerals. International Journal of Mineral Processing, 2004, 74 (Supplement 1), S365-371.

Baláž P., Dutková E., Fine milling in applied mechanochemistry. Minerals Engineering, 2009, 22 (7-8), 681-94.

Borda M.J., Elsetinow A.R., Schoonen M.A., Strongin D.R., Pyrite-induced hydrogen peroxide formation as a driving force in the evolution of photosynthetic organisms on an early earth. Astrobiology, 2001, 1 (3), 283-8.

Borda M.J., Elsetinow A.R., Strongin D.R., Schoonen M.A., A mechanism for the production of hydroxyl radical at surface defect sites on pyrite. Geochimica et Cosmochimica Acta, 2003, 67, 935-9.

Bryan C.J., Jones G.C., van Wyk N., Tupikina O.V., Harrison S.T.L., van Hille R.P., Development and critical evaluation of techniques for the recovery and analysis of sessile and planktonic microbial populations involved in heap bioleaching. In preparation.

Cohn C.A., Laffers R., Simon S., O' Riordan T., Schoonen M., Role of pyrite in formation of hydroxyl radicals in coal: possible implications for human health. Particle and Fibre Toxicology, 2006, 3, 16.

Dimitrijević M., Antonijević M.M., Dimitrijević V., Investigation of the kinetics of pyrite oxidation by hydrogen peroxide in hydrochloric acid solutions. Minerals Engineering, 1999, 12 (2), 165-74.

Gautier V., Escobar B., Vargas T. Cooperative action of attached and planktonic cells during bioleaching of chalcopyrite with *Sulfolobus metallicus* at 70 ℃. Hydrometallurgy, 2008, 94 (1-4), 121-126.

Halliwell B. Biochemistry of oxidative stress. Biochemical Society Transactions, 2007, 35 (5), 1147-1150.

Hu H, Chen Q, Yin Z, He Y, Huang B. Mechanism of mechanical activation for sulfide ores. Transactions of Nonferrous Metals Society of China, 2007, 17 (1), 205-213.

Imlay JA. Cellular defenses against superoxide and hydrogen peroxide. Annual Review of Biochemistry, 2008, 77, 755-776.

Murphy R, Strongin DR. Surface reactivity of pyrite and related sulfides. Surface Science Reports 2009, 64 (1), 1-45.

Nemati M, Lowenadler J, Harrison STL. Particle size effects in bioleaching of pyrite by acidophilic thermophile *Sulfolobus metallicus* (BC). Applied Microbiology and Biotechnology, 2000, 53 (2), 173-179.

Pourghahramani P, Forssberg E. Effects of mechanical activation on the reduction behavior of hematite concentrate. International Journal of Mineral Processing, 2007, 82 (2), 96-105.

Pourghahramani P, Forssberg E. Microstructure characterization of mechanically activated hematite using XRD line broadening. International Journal of Mineral Processing, 2006, 79 (2),106-119.

Schoonen MA, Cohn CA, Roemer E, Laffers R, Simon SR, O'Riordan T. Mineral-Induced Formation of Reactive Oxygen Species. Reviews in Mineralogy and Geochemistry, 2006, 64 (1),179-221.

Schoonen MAA, Harrington AD, Laffers R, Strongin DR. Role of hydrogen peroxide and hydroxyl radical in pyrite oxidation by molecular oxygen. Geochimica et Cosmochimica, 2010,74 (17), 4971-4987.

Valencia P, Acevedo F. Are bioleaching rates determined by the available particle surface area concentration? World Journal of Microbiology & Biotechnology, 2009, 25, 101-106.

Ye X, Gredelj S, Skinner W, Grano SR. Regrinding sulphide minerals — Breakage mechanisms in milling and their influence on surface properties and flotation behaviour. Powder Technology, 2010, 203 (2), 133-147.

Yue J, Klein B. Particle breakage kinetics in horizontal stirred mills. Minerals Engineering, 2005,18 (3), 325-331.